Powder Technology 482 (2026) 122759

Contents lists available at ScienceDirect

Powder Technology

journal homepage: www.journals.elsevier.com/powder-technology

Plastic flow and stress redistribution in sheared granular gouge

Zhuan Dai [a,b], Ke Gao [a,*]

[a] Department of Earth and Space Sciences, Southern University of Science and Technology, Shenzhen, Guangdong, China
[b] School of Engineering and Technology, Baoshan University, Baoshan, Yunnan, China

HIGHLIGHTS

- The plasticity in granular gouge sheared by deformable plates is analyzed.
- The influence of loading conditions on granular plasticity is studied.
- Stress redistribution resulting from plastic flow of granular gouge is elucidated.

GRAPHICAL ABSTRACT

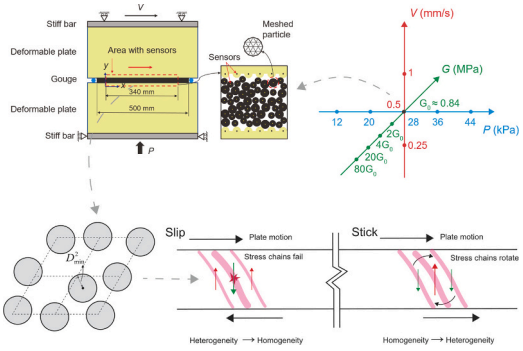

ARTICLE INFO

Keywords:
Sheared granular gouge
Deformable plate
Granular plasticity
Stress redistribution
Non-affine displacement
Loading condition

ABSTRACT

Due to rock grinding and fragmentation, thin layers of granular gouge form between fault surfaces. The plastic flow of granular gouge during stick-slips and the resulting stress redistribution remain unclear. To deepen understanding of the shearing process in faults, this paper employs the combined Finite-Discrete Element Method (FDEM) to simulate the shearing of gouge particles under different loading conditions (i.e., normal stress, shear velocity, and plate stiffness). In small slip events, plastic flow in the gouge is localized due to the failure of only local stress chains. In contrast, during large slip events, more stress chains will fail, leading to a more uniform distribution of plastic flow. In short stick phases, the plastic flow of particles is concentrated in localized areas, triggering new slip events. Conversely, during long stick phases, particle plastic flow is relatively uniform. Higher normal stress, higher slip velocity, and lower plate stiffness result in a more intense plastic flow of the gouge during slip phases, corresponding to faster slip events. Higher plate stiffness leads to more intense particle plastic flow during the stick phase and also reduces the duration of the stick periods. Since similar fault geometries are used, the distributions of normalized particle plastic flow are similar across all loading conditions. During slips, the release of stress on the broken strong force chains causes plate movement, which increases the stress magnitudes of the surrounding stress chains, thereby homogenizing the stress state in the gouge. During stick periods, the strong stress chains accumulate stress and rotate slowly, thickening the gouge and reducing the surrounding stress chains, resulting in a heterogeneous gouge stress state. Our results are valuable for explaining how granular gouge sandwiched between fault surfaces flows during stick-slips and the resulting stress redistribution in 2D fault models.

* Corresponding author.
E-mail address: gaok@sustech.edu.cn (K. Gao).

https://doi.org/10.1016/j.powtec.2026.122759
Received 24 January 2026; Received in revised form 28 May 2026; Accepted 29 May 2026
Available online 1 June 2026

1. Introduction

Granular matter is ubiquitous. Although the motion of an individual granular particle is straightforward, a collection of particles can exhibit complex motion and mechanical response [1]. Understanding how microstructures evolve within the granular mass is crucial for understanding natural phenomena such as grain stacking [2], landslides [3], avalanches [4], dune evolution [5], and debris flows [6]. In particular, thin layers of granular gouge form between fault surfaces due to rock grinding and fragmentation [7–11]. Previous work has demonstrated that the properties of thin granular gouge are closely related to the macroscopic shearing state of a fault [12,13]. Therefore, elucidating microevolution within the granular gouge is crucial for deepening our understanding of the shearing process in natural faults.

Laboratory earthquakes—simulated fault shearing at the laboratory scale—are controllable and repeatable, providing an effective way to explore fault shear processes [14–27]. Existing work has demonstrated that mineral types and their corresponding fault strengths significantly influence fault stability [18]. Such analyses can aid in interpreting the seismic features of natural faults [28,29]. With the aid of scanning electron microscope (SEM) imaging [12,30–32] and X-ray tomography [13,33,34], researchers have characterized the microstructures of granular gouge and linked the microstates within the gouge to the macrostates of faults. Additionally, compared to mineral gouges, adopting photoelastic gouge particles can capture the evolution of stresses inside the granular gouge [35], which also serves as an important experimental method in laboratory earthquakes to probe the mysteries of microstructures inside granular gouges.

With improvements in computational methods and efficiency, numerical simulation is an effective tool for extracting microscopic information that is difficult to obtain in the laboratory [34,36–48]. The Discrete Element Method (DEM) can simulate discontinuous granular materials and is widely used to model sheared granular materials [49,50]. Given the focus on microscopic mechanisms within fault gouge, the shearing plates in DEM models are typically modeled as rigid. Relevant research primarily falls into two categories. (1) How the microscopic properties and constitutive relations of fault gouge influence the macroscopic behavior of faults: Ferdowsi and Rubin [51] discovered that fault healing can occur even when time-independent constitutive relations are used for inter-particle contacts in simulations, suggesting that fault healing can be explained by self-adjustment at the microscopic contact level within fault gouge; Dorostkar and Carmeliet [52] found that the friction coefficient between particles plays a critical role in controlling stick-slip behavior of faults; A higher friction coefficient increases fault strength but shortens the period of stick-slip cycles while reducing the stress drop during each slip event. (2) How the microscopic states of fault gouge evolve under different loading conditions (e.g., varying loading conditions or particle properties): Zou et al. [37] applied different shearing rates to granular materials and used non-affine displacement to quantitatively describe plastic deformations in the material; based on correlations observed, they provided a microscopic explanation for why fault strength initially increases with shearing velocity before stabilizing; Man et al. [53] investigated how particle friction coefficients affect microscopic particle dynamics, revealing that an increase in inter-particle friction coefficient reduces relative velocity fluctuations within the granular system to a certain extent, thereby weakening particle plastic flow.

However, the deformability of the plates directly affects the arrangement of gouge particles, and incorporating deformable shear plates in numerical granular fault models may help capture more realistic microstructures within the granular gouge. Guo and Morgan [54] used elastic and breakable bonds to connect rigid particles, forming sheared bulk materials; they showed how shear bulks are worn and how gouge layers are formed. The calibration of microparameters in DEM is all based on a trial-and-error process. A recently developed numerical method—the combined Finite-Discrete Element Method (FDEM) [49], which merges finite element-based analysis of continua with discrete element-based transient dynamics, contact detection, and contact interaction solutions for discontinua, provides a natural solution for modeling such a fault [55]. Gao et al. [56] employed FDEM to develop a numerical model incorporating deformable shearing plates and circular fault gouge particles; they found that the magnitude of fault slip velocity is directly proportional to the normal stress and inversely proportional to the square root of the shear modulus of the shearing plates, whereas the shearing rate has minimal influence on slip velocity. Based on the simulation data from Gao et al. [55], Zhang et al. [57] conducted a statistical analysis of the stress tensor within the fault gouge during stick-slip cycles; they discovered that small slip events tend to increase the heterogeneity of stress distribution in the fault gouge (with only localized self-adjustment occurring); in contrast, large slip events result in a more uniform stress distribution (with self-adjustment occurring through the entire fault gouge). Researchers have begun not only validating numerical models of faults through practical experiments but also continuously improving simulation models. Mollon et al. [58] proposed a numerical model for simulating stick-slip cycles: the rock mass is represented as a continuous elastic medium, while the shear zone is depicted using irregular, deformable particles.

Unlike continuous solids, the discrete gouge particles can easily slide or rotate relative to one another. The “non-affine displacement” has been shown to be an effective tool for quantifying granular plasticity, which is closely related to the macroscopic evolution of granular materials [59]. With the aid of the non-affine displacement, Ma et al. [60] studied the temporal evolution of the spatial correlation of granular plasticity, and Cao et al. [34] illustrated the accompanying topology change. Mei et al. [61] found that, using non-affine displacement as input, the macro stress increase or decrease in stick or slip phases can be predicted by a machine learning method (3D convolutional neural network), indicating that non-affine displacement is also an effective method for depicting micro dynamics.

The granular gouge deforms plastically, which will definitely result in stress redistribution. However, how particles flow and how stress is redistributed in the stick-slip phases are poorly understood, which is essential for understanding the complex evolution mechanism of faults that undergo stick-slip cycles [62–65]. A systematic study of how loading conditions influence the plasticity of granular gouge sheared by deformable plates and how this plasticity relates to stress redistribution remains lacking. In this paper, we simulate sheared granular gouges with deformable plates using FDEM. The granular plasticity is characterized by the non-affine displacement, and slip events and stick periods are extracted. We demonstrate how granular plasticity accumulates during stick-slip cycles and how different loading conditions (e.g., normal stress, shear velocity, and plate stiffness) influence its accumulation. Finally, we examine stress redistribution in the granular gouge during stick-slip cycles.

2. Methods

2.1. FDEM and model setup

The FDEM was initially conceived by Munjiza in the early 1990s and designed to model the transition of solid materials from a continuous to a discontinuous state, as well as the intricate interactions among discrete solid bodies [49]. Within the FDEM framework, the finite element method (FEM) component handles deformation calculations for continuous objects, while the discrete element method (DEM) component supports precise contact detection and interaction processing, enabling the capture of complex dynamics between discrete and continuous objects. By combining the strengths of both FEM and DEM, FDEM excels in simulating granular fault systems. The FDEM-based granular fault model integrates with deformable plates to simulate gouge shearing, generating characteristic stick-slip cycles and providing insights into the intricate stress evolution within the gouge. For a

comprehensive understanding of FDEM, readers are referred to our prior publications [55,56,66].

Using FDEM, we recreate a two-dimensional fault system with a granular gouge, inspired by the photoelastic experiments of Geller et al. [67], as previously explored in Gao et al. [55]. To hinder crystallization during shear, we use a bimodal diameter distribution (1.2 or 1.6 mm, equally distributed) for the circular gouge particles, following recommendations from Tsai et al. [68]. Each particle is meshed into 24 nearly uniform triangular finite elements to precisely capture its deformation. This gouge is positioned between two identical deformable plates, as illustrated in Fig. 1. A consistent shear velocity is imparted to the upper rigid bar to simulate fault shearing, while a steady normal load is maintained on the lower rigid bar. Constrained movement is enforced, with the top bar permitted only x axis motion and the bottom bar restricted to y axis motion.

Following consolidation, the gouge measures 500 mm in length and approximately 11 mm in thickness. To facilitate shearing, the plate boundaries feature semicircular "teeth" with a diameter of 1.6 mm. Within the model's central section (highlighted by the red dashed rectangle in Fig. 1a), we place "sensors" at the teeth and particle centers. Data on displacement, velocity, and stress tensors are recorded at each sensor point every millisecond. A total of 1917 particles with sensors are integrated, accompanied by 143 sensors on both the top and bottom plates. The reference model utilizes parameters such as a normal stress of 28 kPa, a shear velocity of 0.5 mm/s, and a plate shear modulus of 0.84 MPa. Then we vary the normal stress (12 kPa, 20 kPa, 28 kPa, 36 kPa and 44 kPa), shear velocity (0.25 mm/s, 0.5 mm/s, 1 mm/s) and plate shear modulus (G_0, $2G_0$, $4G_0$, $20G_0$ and $80G_0$, G_0 = 0.84 MPa) respectively to explore how these loading conditions (Fig. 1b) influence the microstates in granular faults. It has been proven that these three parameters can significantly influence the shear behavior of faults [12,69,70]. Model parameters are outlined in Table 1.

Before entering standard stick-slip cycles, the numerical model undergoes a phase of consolidation and pre-shear. Shearing initiates once the system reaches equilibrium after consolidation (when the kinetic energy stabilizes to nearly zero). The inertial number of the model ($I = \dot{\gamma}d/\sqrt{P/\rho}$) is between 10^{-6} and 10^{-4} (much smaller than 10^{-3}), indicating that the system is in a quasi-static shearing state. Here, $\dot{\gamma}$ is the shear rate, d is the particle's average diameter, P is the normal pressure, and ρ is the particle's density. $\dot{\gamma}$ is calculated by

$$\dot{\gamma} = \frac{V}{H_g}, \tag{1}$$

where H_g is the thickness of the granular gouge (~11 mm). In our previous work, we calibrated the simulated results to ensure that the magnitudes of the generated slip events align appropriately with the Gutenberg-Richter distribution [55].

Table 1
Numerical simulation parameters [56].

Property	Value	Property	Value
Particle diameter	1.2 or 1.6 mm	Stiff bar density	2,800 kg/m^3
Particle density	1,150 kg/m^3	Stiff bar Young's modulus	30 GPa
Particle Young's modulus	10 MPa	Stiff bar Poisson's ratio	0.33
Particle Poisson's ratio	0.4	Foam density	1,150 kg/m^3
Particle-particle friction coefficient	0.15	Foam Young's modulus	1 MPa
Total particle number	2,817	Foam Poisson's ratio	0.4
Number of particles with sensors	1917	Contact penalty	4 GPa
Main plate density	1,150 kg/m^3	Time step	1.0E-7 s
Main plate shear modulus	0.84–67.2 MPa	Normal load P	12–44 kPa
Main plate Poisson's ratio	0.49	Shear velocity V	0.25–1 mm/s
Particle-plate friction coefficient	0.15	Teeth diameter	1.6 mm

2.2. Characterization of granular plasticity

The granular plasticity of a particle is defined as the dislocation between the particle and its neighbors. Quantifying granular plasticity can be an effective way to demonstrate where gouge motion is more pronounced during stick-slips. In the meantime, stress redistribution in these areas can be studied to further validate the results. Specifically, the plasticity in granular gouge can be characterized by the non-affine displacement [60]. Here, the non-affine displacement of a particle is the deviation of the particle's position from the best-fit affine transformation over the time window Δt, i.e.,

$$D^2_{\min}(t,\Delta t) = \frac{1}{N_i}\sum_{j}^{N_i}\left|\mathbf{r}_j(t+\Delta t) - \mathbf{r}_i(t+\Delta t) - \mathbf{J}\left[\mathbf{r}_j(t) - \mathbf{r}_i(t)\right]\right|^2, \tag{2}$$

where the subscript i denotes the designated particle, and the index j iterates over its N_i neighbors within a cutoff distance w relative to the reference particle i at $\mathbf{r}_i(t)$ (the position of particle i at time t). Here, t is a time stamp during shear, and $\mathbf{J}$ is the best-fit affine transformation tensor that minimizes the quantity $D^2_{\min}$. $\mathbf{J}$ can be calculated using the following equations:

$$\mathbf{X} = \sum_{j}^{N_i}\left[\mathbf{r}_j(t+\Delta t) - \mathbf{r}_i(t+\Delta t)\right] \otimes \left[\mathbf{r}_j(t) - \mathbf{r}_i(t)\right], \tag{3}$$

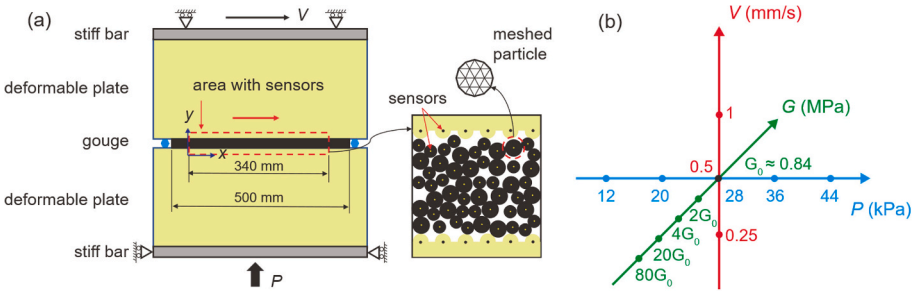

Fig. 1. Model setup and selection of key simulation parameters. (a) Model setup. The gouge is sandwiched between two identical deformable plates. Each particle is further meshed into 24 triangular elements. There are 1917 particles with sensors, and an additional 143 sensors are located on each of the top and bottom plates near the gouge. (b) Selection of key simulation parameters: normal load P (first group, blue), shear velocity V (second group, red), and plate shear modulus G (third group, green). (For interpretation of the references to colour in this figure legend, the reader is referred to the web version of this article.)

$$\mathbf{Y} = \sum_{j}^{N_i} \left[\mathbf{r}_j(t) - \mathbf{r}_i(t)\right] \otimes \left[\mathbf{r}_j(t) - \mathbf{r}_i(t)\right], \tag{4}$$

$$\mathbf{J} = \mathbf{X} \cdot \mathbf{Y}^{-1}. \tag{5}$$

Here, $D^2_{\min}(t, \Delta t)$ can be deemed as the accumulation of particle dislocation in the gouge from t to $t + \Delta t$ and also indicates the shear localization in the gouge. The physical meaning of $D^2_{\min}$ is shown in Fig. 2. The deviation of a particle's displacement from affine displacement is the non-affine displacement $D^2_{\min}$ of the particle, which quantifies the particle's plasticity (i.e., the degree of deviation from purely elastic deformation).

Here, to characterize granular plasticity during stick-slip cycles, for each stick-slip period, time windows (from t to $t + \Delta t$) are set from the start to the end of each slip event or stick period. The larger the neighbor cutoff distance w, the more particles will be designated as neighbor particles. Consequently, $D^2_{\min}$ will show a more homogeneous distribution pattern and reflect fewer local features. On the other hand, the smaller w is, the fewer particles will be designated as neighbor particles, and the $D^2_{\min}$ will show more heterogeneous distribution patterns and reflect more local features. Here, the w is set to 2 mm, ensuring that w is neither too large to reflect local features nor too small to allow particles nearby to be assigned.

2.3. Characterization of slip events

In each loading scenario, the simulated granular fault generates slip events exhibiting diverse characteristics. To investigate granular plasticity during stick-slip cycles, we identify and characterize these events to illustrate the macroscopic properties of sheared granular faults. The extraction process involves the following steps. (1) Timestamp Classification: Establish a threshold $v_{\text{thresh}} = 0.001$ m/s (which is selected by a series of tests and distinguishes the slip events well and does not interrupt the basically increasing stick phase); the timestamps in which the plate differential velocity $|\Delta v_p|$ (half the absolute difference between top and bottom plate velocities) exceeds v_{thresh} are classified as slip phase; otherwise, they are classified as the stick phase. (2) Timestamp Connection: A sequence of consecutive timestamps in the slip phase (uninterrupted by stick phase timestamps) is connected to constitute a distinct slip event; temporarily, the first timestamp marks its start, and the last timestamp marks the end of the event. (3) Event Extension: Based on the rate of the change of $|\Delta v_p|$ at the beginning or end of a slip event, we estimate the points where $|\Delta v_p|$ rises from 0 and falls to 0; these timestamps are designated as the new start and end of the slip event, respectively. (4) Slip Event Merging: After extension, overlapping timestamps may occur between slip events; we merge these overlapping events into a single new event, and use the earliest start of the merged events as the new start and the latest end as the new end. Then, we remove the merged events and retain the new consolidated events.

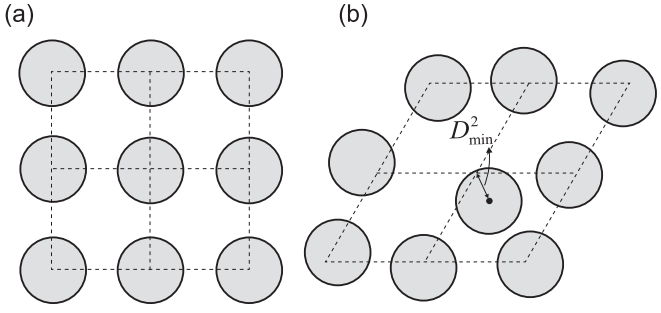

Fig. 2. Illustration of granular plasticity. (a) Assumed particle arrangement before shear, and dashed lines show the overall shape of the granular mass. (b) Particle arrangement after disturbance, and dashed lines show the overall shape (the overall shape in (a) after affine deformation); the deviation of a particle's displacement from affine displacement is the non-affine displacement $D^2_{\min}$ of the particle.

The seismic moment serves as a reliable indicator of the scale of slip events, and we use it to characterize these events. Specifically, the seismic moment for a slip event is defined as

$$M_0 = GDS, \tag{6}$$

where G is the shear modulus of the shear plates; D is the accumulated plate differential displacement (the absolute value of the difference between the top and bottom plate in terms of their respective average displacement) during the slip event; S is the area of the fault plane, which is the length of the gouge times unity (assuming unit length perpendicular to the 2D fault model).

3. Results

3.1. General results

To depict the general results of the simulated granular gouges subjected to various loading conditions, we define the shear force as the average absolute value of the contact force between the gouge mass and the two plates. The average x velocities of the top plate (V_{pt}, ranging from ~0 to ~0.025 m/s) and the bottom plate (V_{pb}, ranging from ~ −0.025 to ~0 m/s) are respectively taken as the average x velocities of the 143 sensors on the top and bottom plates. In the stick phase, the gouge locks the shear plates, the shear plates move at a velocity around half the shear velocity (~$1.25–0.5 \times 10^{-3}$ m/s), but the V_{pt} is slightly larger than V_{pb} due to the accumulation of shear strain in the granular gouge. In the slip phase, the gouge unlocks, and the elastic energy is released. The elastic rebound of the plates makes the V_{pt} and V_{pb} evolve in opposite directions and become nearly symmetric. Detailed analysis of plate motion can be found in Gao et al. [56].

Here, we focus on the shearing stage when the shear forces are stabilized. Fig. 3 shows the evolution of shear force and plate velocity under different loading conditions; each column represents the sheared granular gouge under different normal stresses, shear velocities, and shear modulus of the plates, respectively. Then, the slip events in the stable shearing stages of these numerical simulations are extracted (see the Methods section). Their properties are illustrated in Fig. 4 and Fig. 5.

In models subjected to different normal stresses, higher normal stresses often result in higher shear force during the stable shearing stage (Fig. 3a). With increased normal stress, the shear force increases from ~2 kN to ~7 kN. The slip mode is also strongly influenced by the normal stress (Fig. 3b). With increased normal stress, the sheared faults exhibit more pronounced stick-slip cycles. Higher normal stresses also result in larger stress drop events and more pronounced plate motion during slips (Fig. 3b). The slip events exhibit higher slip velocities in models with higher normal stress (Fig. 4a; the fitted curve has a steeper slope at higher normal stress). The complementary cumulative distribution function also tells that events have large seismic moments when the normal stress is higher (Fig. 5a). To sum up, higher normal stresses facilitate the locking of granular gouge and fault planes, allowing longer stick phases to store more elastic energy and produce quicker events [14,43,70,71].

The shear velocity has a slight influence on the slip mode. All models at different shear velocities undergo stick-slip cycles upon entering the stable shearing stage (Fig. 3c and d). However, slip events occur at a higher frequency when the shear velocity is higher (Fig. 3d), and they also exhibit a slightly faster slip velocity and longer duration (Fig. 4b, slightly wider distribution range for faster shear velocities). Correspondingly, the seismic moments of the slip events are slightly higher when the shear velocity is higher (Fig. 5b).

Shear modulus of the shear plates influence the macroscopic properties of the fault a lot (Fig. 3e). High shear modulus allow the shear

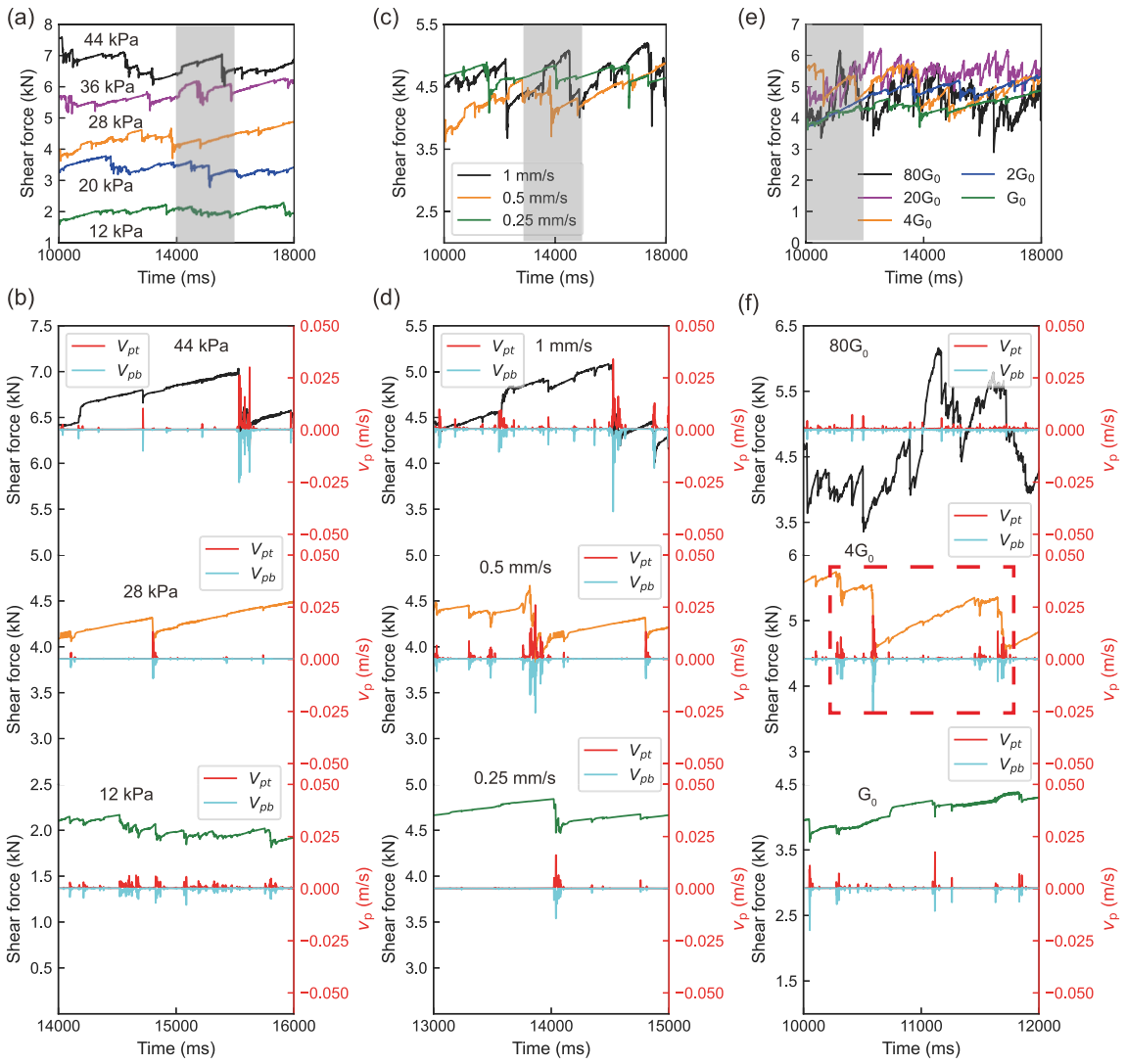

Fig. 3. General simulation results. (a) The evolution of shear force for models under different normal stresses. (b) Enlarged details for the period from time = 14 000 ms to 16 000 ms highlighted in grey in (a). (c) The evolution of shear force for models under different shear velocities. (d) Enlarged details for the period from time = 13 000 ms to 15 000 ms highlighted in grey in (c). (e) The evolution of shear force for models with different plate stiffness. (f) Enlarged details for the period from time = 10 000 ms to 12 000 ms highlighted in grey in (e).

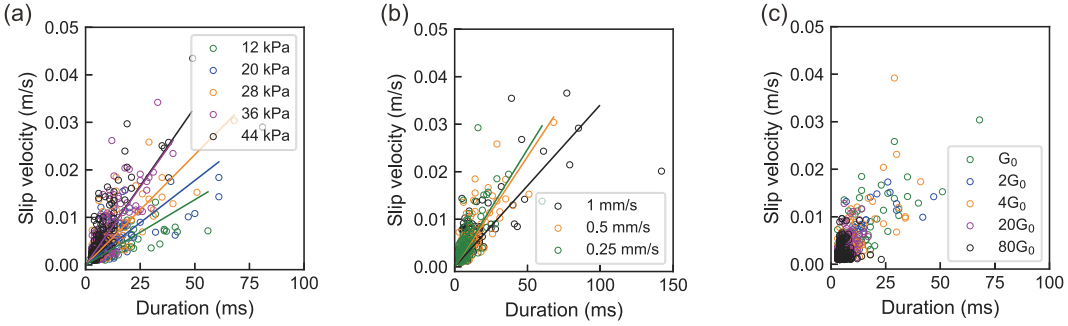

Fig. 4. The slip velocity versus the duration of each slip event. (a) Slip events under different normal stress. (b) Slip events under different shear velocities. (c) Slip events under different plate shear modulus.

force to oscillate during the stable shearing stage, and the plate velocities are slow during slips. On the contrary, the sheared fault undergoes regular stick-slip cycles when the shear modulus are low (Fig. 3f). Both the slip velocity and duration of slip events decrease with the increase of shear modulus (Fig. 4c, a much narrower distribution range for stiff shear plates). However, when taking the properties of the shear plates into account, there are events with larger seismic moments with the increase of shear modulus according to the complementary cumulative distribution function of the seismic moment (Fig. 5c). Based on the rate-and-state friction law [72], the rise of stick-slip can be attributed to the

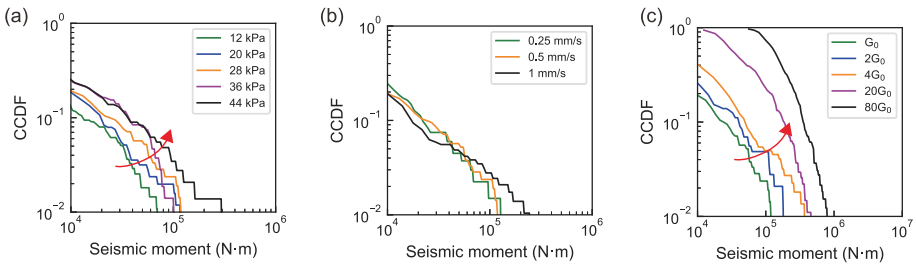

Fig. 5. The complementary cumulative distribution function (CCDF) of seismic moment of slip events. (a) Slip events under different normal stresses. (b) Slip events under different shear velocities. (c) Slip events under different plate shear modulus.

competition between the loading stiffness and the rheologic stiffness (determined by the normal stress and the properties of the frictional surface). In small-scale laboratory earthquakes, plate deformation is negligible, and low loading stiffness facilitates the accumulation of elastic energy during the stick phase, leading to larger slip events [43,70]. However, here, stiff shear plates produce larger events, which may be explained by the fact that stiff shear plates are more prone to cause the slip of the whole fault plane in the slip phase compared to the soft ones. Additionally, it is not difficult to imagine that with a further increase in the shear modulus, the plates will become rigid and slide stably.

3.2. Granular plasticity during shearing

To describe the evolution of granular plasticity in the gouge during shearing, we first select two typical slip events in the model with $P = 28$ kPa, $V = 0.5$ mm/s, and $G = 4G_0$ to illustrate how granular plasticity accumulates during slip phases. The two selected slip events are marked in Fig. 6 (also highlighted by the dashed red rectangle in Fig. 3f). One is a small slip with a much smaller stress drop and $|\Delta v_p|$ than the other large slip. The accumulated granular plasticity during the two events is shown by the non-affine displacement (D^2_{min}) in Fig. 7. For the small slip, the granular plasticity is localized, meaning that only minor rearrangements of local supporting structures are required (Fig. 7a). For the large slip, the granular plasticity concentrates in several areas, indicating a higher likelihood of failure in the supporting structures within the granular gouge (Fig. 7b). The average normalized non-affine displacement ($D^2_{min}/\langle D^2_{min}\rangle$) of each layer along the x and y axes also indicates that small slips have a more localized granular plasticity (Fig. 7).

To illustrate the accumulation of granular plasticity in the stick phase, two stick periods from the same model marked in Fig. 6 are also selected. One is a short stick period that accumulates less shear force before slip, and the other is a long stick that accumulates more shear force before slip. The accumulated granular plasticity during the two periods is also evident in the non-affine displacement (D^2_{min}) presented in Fig. 8. For the short stick, the granular plasticity is more localized, meaning the gouge particles there are not well locked after slip, and small localized slips between unlocked particles can trigger subsequent slip events (Fig. 8a). For the long stick, the granular plasticity appears homogeneous, indicating that the granular gouge confines and locks each other well and thus more shear forces are accumulated (Fig. 8b).

Therefore, granular plasticity accumulates in both slip and stick phases. We also find that after a long-term shearing, granular plasticity witnesses a relatively homogeneous distribution (Fig. 9). This is likely because, in the long-term shearing process, each part of the continuous plates drags or pushes its neighbors, causing them to move together; thus, granular plasticity along the x axis shows a homogeneous distribution (Fig. 9). However, during slips, even in large events, granular plasticity concentrates in several areas, and the short stick period further localizes it. Due to the driving force of the plate, the supporting structures and the stress distribution in the granular gouge evolve during each slip. Thus, the homogeneous distribution of long-term granular plasticity along the x axis results from the superposition of heterogeneous distributions within each slip event and stick period. Along the y axis, granular plasticity is lower near the plates because they are more confined by the plates.

3.3. Effects of loading condition on granular plasticity

As shown in Fig. 10, we use the complementary cumulative distribution function (CCDF) of non-affine displacement (D^2_{min}) to compare the granular plasticity under different loading conditions. Taking the two typical slip events and the two stick periods studied in Section 3.2 as examples, the CCDFs of the large slip and the long stick are higher than those of the small slip and short stick, respectively (Fig. 10a and b), indicating more accumulated granular plasticity in the large slip and long stick than their counterparts. Then, we extract all slip events and stick periods in all models under different loading conditions after the shear faults enter a stable shearing state. The CCDFs of granular plasticity for each slip event and stick period in each model are calculated. The model with higher normal stresses tends to accumulate more granular plasticity during slip events due to faster slip rates (Fig. 10c).

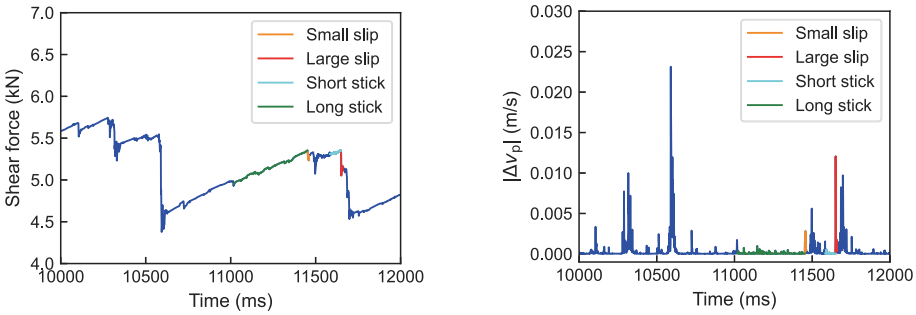

Fig. 6. Four typical periods: small slip, large slip, short stick, and long stick. These typical periods are taken from the case with $P = 28$ kPa, $V = 0.5$ mm/s, and $G = 4G_0$ (marked by the dashed red rectangle in Fig. 3f). (For interpretation of the references to colour in this figure legend, the reader is referred to the web version of this article.)

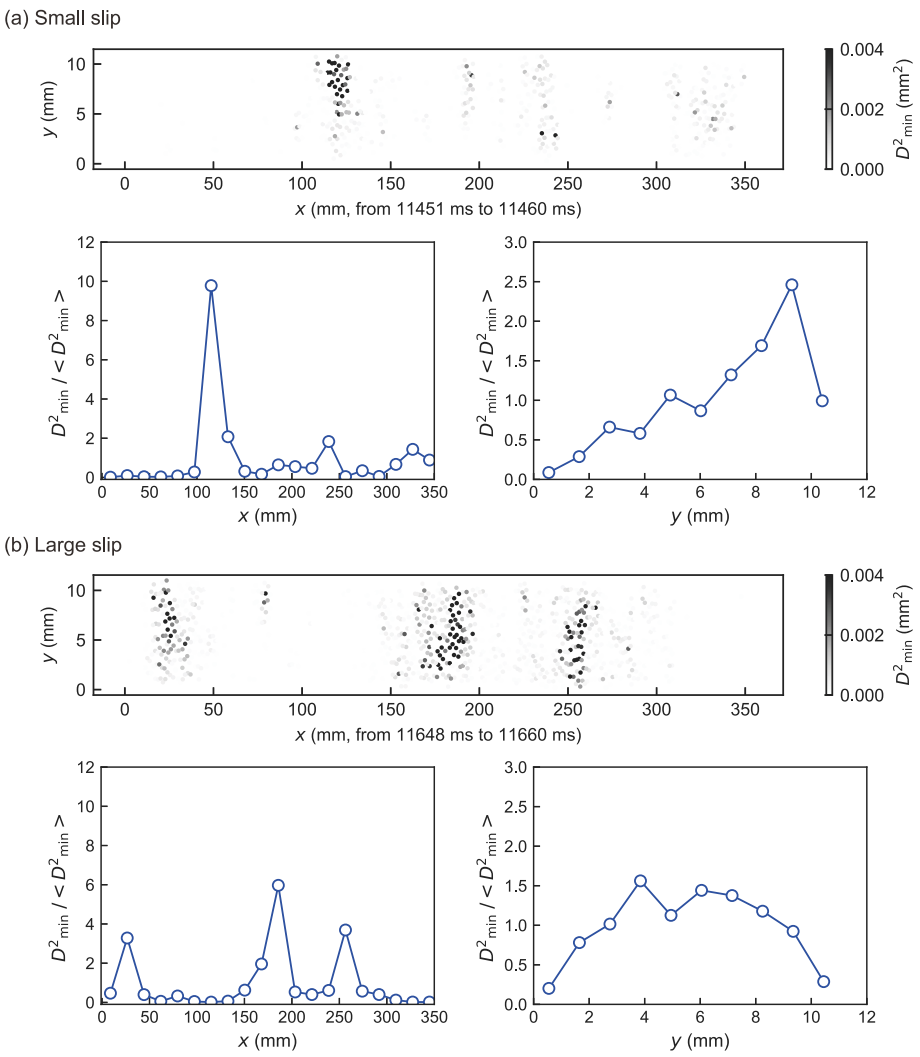

Fig. 7. Non-affine displacement during slips. The two examples are taken from the model with $P = 28$ kPa, $V = 0.5$ mm/s, and $G = 4G_0$, which are marked in Fig. 6. (a) Accumulated non-affine displacement in the small slip event, and (b) the accumulated non-affine displacement in the large slip event. Figures at the lower left and right show the average normalized non-affine displacements along the x and y axes, respectively.

However, the granular plasticity in the stick phase under different normal stresses is similar (Fig. 10f), although stick phases are more prominent and longer in the model with higher normal stresses (Fig. 3b). This similarity could be explained by the increased normal stresses on the particle interlock during the stick phases. Under higher shear velocity, the accumulated granular plasticity in slip events tends to be slightly higher (Fig. 10d) due to the slightly faster and longer slip events (Fig. 4b and Fig. 5b). In contrast, the granular plasticity under different shear velocities is similar in stick phases (faster shear velocity provides a stronger drive for granular flow, but the stick phase is short in time) (Fig. 10g). Because the higher shear modulus of plates result in lower slip velocities and durations of slip events (Fig. 4c), although they have a larger seismic moment (Fig. 5c), models with higher shear modulus accumulate less granular plasticity during slips (Fig. 10e) and more granular plasticity in stick period due to the restriction of stiff plate on the flow of granular gouge (Fig. 10h).

We also calculate the CCDFs of normalized non-affine displacement ($D^2_{\min}/\langle D^2_{\min}\rangle$, i.e., $D^2_{\min}$ normalized by the average $D^2_{\min}$ in the corresponding slip or stick period). Although the CCDFs of $D^2_{\min}/\langle D^2_{\min}\rangle$ are different in large slip, small slip, short stick and long stick (Fig. 11 a-b), in all loading conditions, the CCDFs collapse into a similar pattern in both the slip and stick phases (Fig. 11 c-d). The same geometric structure across all models may cause this kind of similarity [73]. Particle dislocation in the same fault geometry under different loading conditions shows a similar distribution after normalization.

3.4. Plate motion and microdynamics in gouge subject to different plate stiffness

The stiffness of the shear plates can significantly influence the shear behavior of faults, as we show in Section 3.1. Here, to provide a more quantitative analysis of plate motion and microdynamics in gouge subject to different plate stiffness, we first show how the absolute x velocities of sensors on the top plate ($|V_{xt}|$) and bottom plate ($|V_{xb}|$) evolve (Fig. 12a and b). The general dynamics of these two periods are shown in Fig. 3f, and the two periods are taken from the model with $P = 28$ kPa, $V = 0.5$ mm/s, and $G = 4G_0$ (soft shear plate) and the model with $P = 28$ kPa, $V = 0.5$ mm/s, and $G = 80G_0$ (stiff shear plate), respectively. Then, we analyze granular plastic flow during typical slip events in these two periods (Fig. 12c and d).

Compared with the soft plate (Fig. 12a), the distribution patterns of $|V_{xt}|$ and $|V_{xb}|$ of the model sheared by stiff plates (Fig. 12b) have finer lines that span across the entire fault plane. In the velocity cloud map of the model sheared by stiff plates, the number of lines is also more, and the lines are more continuous and less dashed-like. This plate motion indicates the plates tend to move synchronously in a shorter time in the

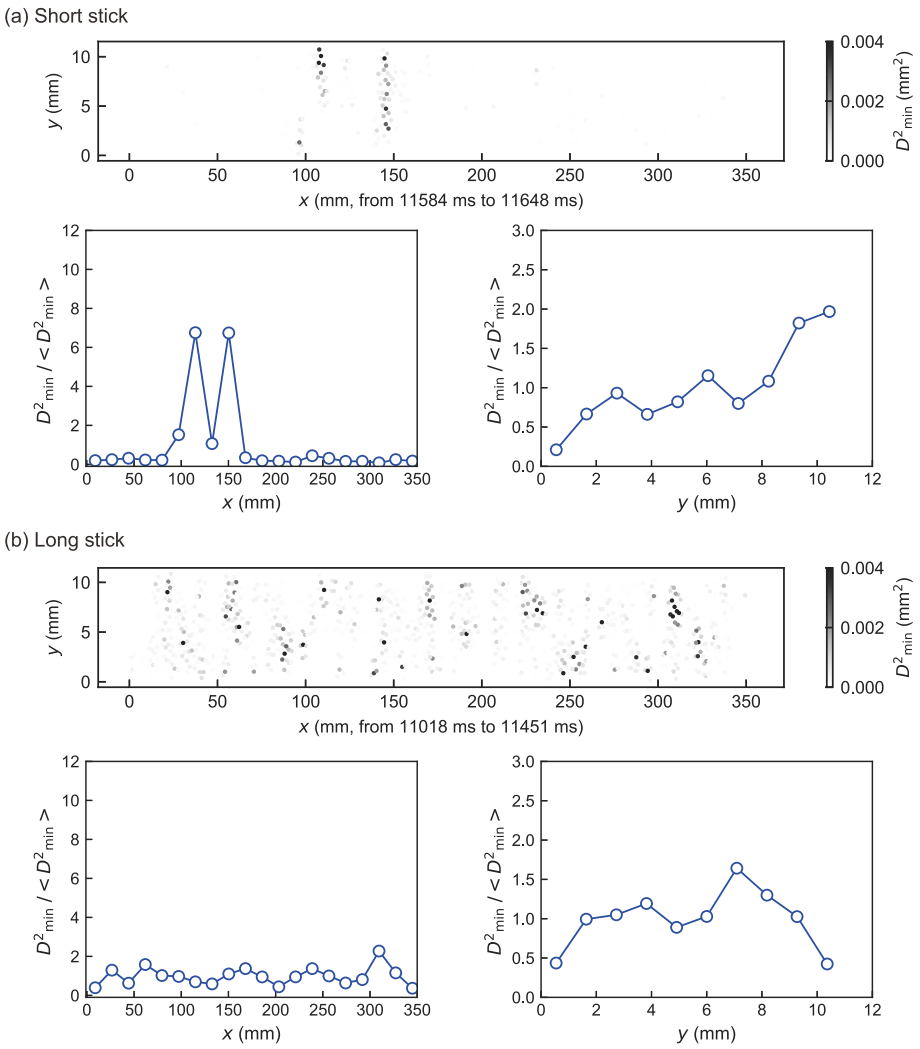

Fig. 8. Non-affine displacement in stick phases. The two examples are taken from the model where $P = 28$ kPa, $V = 0.5$ mm/s, and $G = 4G_0$, marked in Fig. 6. (a) Accumulated non-affine displacement in a short stick period, and (b) accumulated non-affine displacement in a long stick period. Figures at the lower left and right show the average normalized non-affine displacements along the x and y axes, respectively.

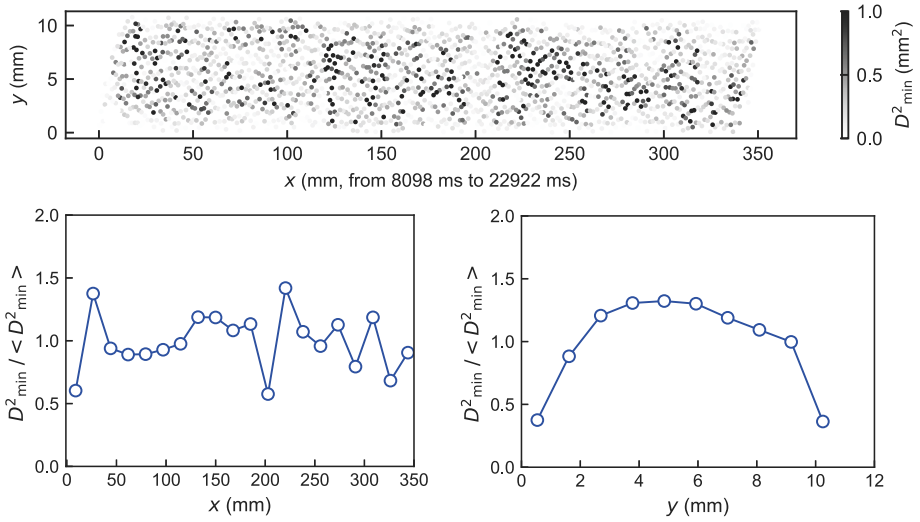

Fig. 9. Long-term non-affine displacement. The model where $P = 28$ kPa, $V = 0.5$ mm/s, and $G = 4G_0$ is taken as an example here. The upper figure shows the spatial distribution of non-affine displacement. The figures at the lower left and right show the average normalized non-affine displacements along the x and y axes, respectively. For the long-term non-affine displacements under different load conditions, see Fig. S1, Fig. S2 and Fig. S3.

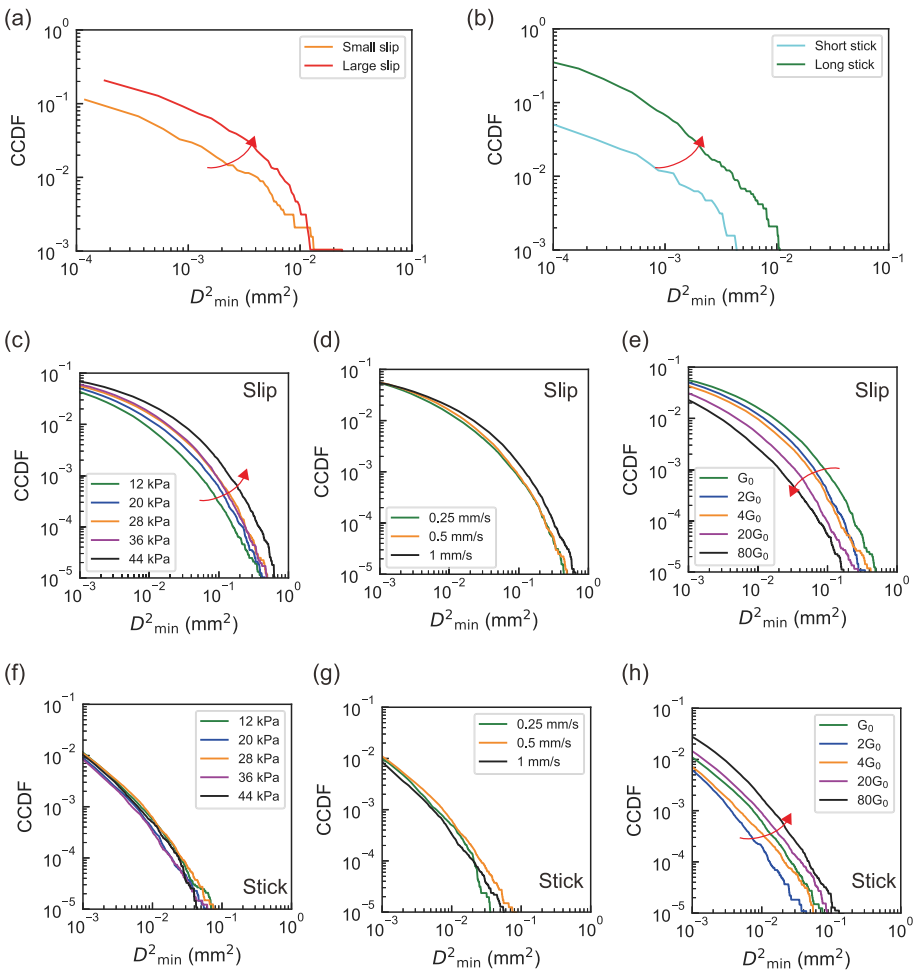

Fig. 10. The complementary cumulative distribution function (CCDF) of non-affine displacement (D^2_{min}). (a) The two slip events shown in Fig. 7. (b) The two stick periods shown in Fig. 8. (c) – (e) Extracted slips of the sheared granular faults under different normal stresses, shear velocities, and plate stiffness, respectively. (f) – (h) Extracted sticks of the sheared granular faults under different normal stresses, shear velocity, and plate stiffness, respectively.

model sheared by stiff plates. However, we check all granular plastic flow of the slip events shown in Fig. 12a and b, the granular plastic flow is more localized in slip events of the model sheared by stiff plates compared to the gouge sheared by soft plates, and the plastic flow of granular gouge in the model sheared by stiff plates is less related to the plate motion. Typical plastic flow of slip events is shown in Fig. 12c and d. Therefore, we infer that when sheared by stiff plates, uneven loading is more prone to occur, leading to a dramatic increase in local stress and subsequent local failure (or local plastic flow). A more quantitative study of the spatial distribution of plastic flow and its relation to plate motion in granular gouge sheared under different plate stiffnesses will be carried out in the future.

4. Discussion

4.1. Accompanied stress redistribution of plastic flow

We have quantitatively studied the plastic granular flow. The plastic granular flow inevitably induces a change in stress within the granular mass, which may influence fault shear processes and is crucial to understanding the accompanying phenomenon. In this section, we further explore and explain the stress change caused by granular plastic flow.

The accumulation and release of shear force along the fault plane during stick-slip cycles are much less than the peak shear force. In addition, the stresses are redistributed in the gouge during both stick and slip phases, with regions of increased and decreased stress present in each phase. Fig. 13 and Fig. 14 show the non-affine displacement (D^2_{min}), stress change ($\Delta\tau$, representing the change in maximum stress over a period), and maximum stress (τ) in the granular gouge of the two slip events and two stick phases we studied in Section 3.2. In the two slip events (Fig. 13a, b, d, and e), larger D^2_{min} results in more dramatic stress changes in these areas, and the stress increase and decrease regions are interlaced in these areas. We also find that areas with larger D^2_{min} correspond to regions with relatively high stresses (Fig. 13c and f). Although in the stick phase the stress increase region and stress decrease region are also interlaced (Fig. 14b and e), we observe a less pronounced connection between the areas with higher D^2_{min} and higher stress (Fig. 14a, c, d, and f).

To establish a more quantitative relationship between $\Delta\tau$ and D^2_{min}, we extract all slip events and stick periods (see Methods) from the stable shearing stage of the model where $P = 28$ kPa, $V = 0.5$ mm/s, and $G = 4G_0$. Then, the two-dimensional probability density of $\Delta\tau$ and D^2_{min} is estimated by kernel density estimation (Text S1). The normalized probability density (normalized by the maximum value) and covariance error ellipse (Text S2) of the discrete data are shown in Fig. 15. Fig. 15a and b show all particles in slips and sticks, respectively. We define the particles that comprise the top 10% τ as those on stress chains. The covariance error ellipses for particles on stress chains deviate from the coordinate axis, indicating that the stress change has a relationship with D^2_{min} when particles are on stress chains. As we mentioned in the last paragraph, at least for slip events, larger D^2_{min} results in more dramatic

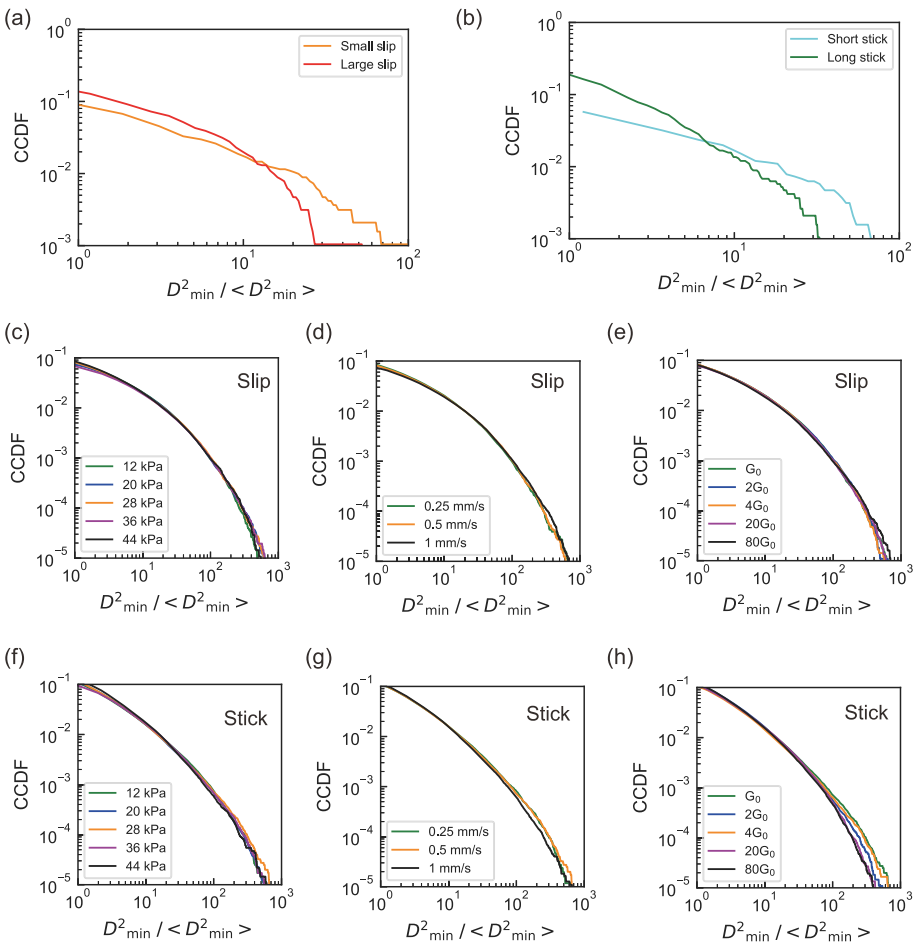

Fig. 11. The complementary cumulative distribution functions (CCDF) of normalized non-affine displacement ($D^2_{min}/\langle D^2_{min}\rangle$). (a) The two slip events shown in Fig. 7. (b) The two stick periods shown in Fig. 8. (c) – (e) Extracted slips of the sheared granular faults under different normal stresses, shear velocities, and plate stiffness, respectively. (f) – (h) Extracted sticks of the sheared granular faults under different normal stresses, shear velocities, and plate stiffness, respectively.

stress changes. Since stress chain structures play a primary role in supporting the plates, to clearly study the relationship between $\Delta\tau$ and D^2_{min}, we neglect the particles that barely flow and consider only the top 10% particles with the largest D^2_{min} in each slip event or stick period (Fig. 15c and d). In both stick and slip phases, the $\Delta\tau$ for particles on stress chains have a much larger range, and $\Delta\tau$ tend to decrease with the increase of D^2_{min}. The covariance error ellipse for particles on stress chains is narrower during slip events than during stick periods, indicating a stronger correlation between stress change and plastic flow during slip events.

Apart from the chain-like structures in stress distribution, the stress changes also exhibit a chain-like distribution (Fig. S4 and Fig. S5). Therefore, stress redistribution during stick-slip is closely related to the stress chain structure. Combined with the interlaced distribution of stress changes, we present a diagram to illustrate stress redistribution during stick-slip cycles (Fig. 16). When a strong stress chain fails, slip events occur, reducing the stress on that chain. The induced plate motion then strengthens the nearby stress chains, resulting in a more homogeneous stress state in these areas. On the contrary, in stick phases, some stress chains rotate slightly to support the plates, and stresses are built up on them. This thickens the gouge, and the stress near the rotating stress chains decreases; thus, the stresses in these areas become more heterogeneous.

Previous researchers have quantitatively investigated the spatial evolution of stress chains through both laboratory experiments and numerical simulations. Daniels and Hayman [35] sheared photoelastic particles and observed differences in force chains before and after slips; they concluded that the force chain structure plays a key role in shear zone deformation. Gao et al. [55] showed that the granular gouge thickens during stick but thins during slip, and that the dip angles of stress chains are roughly aligned in directions that can resist shear and normal loads [66]. Dai and Gao [46] conducted statistical analyses of gouge particle displacement in the stick and slip phases and showed the evolution of stress chains during stick slips. These conclusions all support the evolution of stress chains in Fig. 16.

Quantitative statistical analysis has also been conducted on the evolution of stress heterogeneity in sheared granular gouge. Zhang et al. [57] conducted statistical analyses of stress heterogeneity within a granular fault during stick-slip cycles, finding that it increases during the stick phase; this trend can be explained by the evolution of stress chain, as shown in the stick part of Fig. 16; they found that stress heterogeneity decreases during large slip events. This can also be explained by the evolution of the stress chain shown in the slip part of Fig. 16. However, when small slip events occur, they found that the stress heterogeneity increases. This may be explained by the fact that small slip events occur due to the failure of a local, weaker stress chain, and induced plate motion increases the stresses on the strong stress chain.

4.2. *Implications and limitations*

Constrained by the geometric limitations of laboratory scale, our findings may not fully elucidate the concurrent stress redistribution observed in catastrophic natural earthquakes. For instance, the 2025 Mw 7.8 Myanmar earthquake [74,75], where coseismic slips between fault surfaces extended to a meter scale (~6 m). In contrast, even within

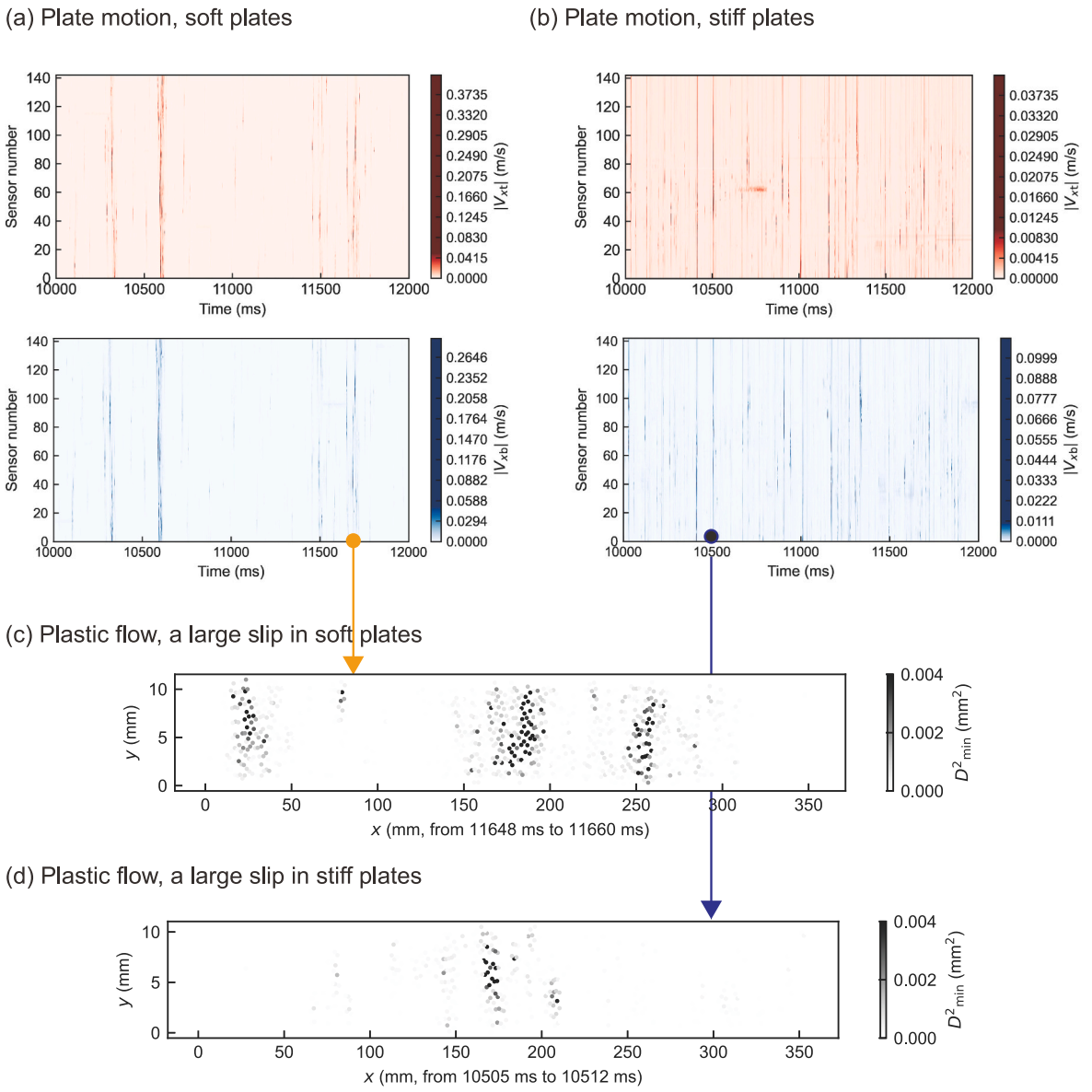

Fig. 12. Plate motion and plastic flow in gouge subject to different plate stiffness. The plate motion is taken from the model with $P = 28$ kPa, $V = 0.5$ mm/s, and $G = 4G_0$ (soft shear plate) and from the model with $P = 28$ kPa, $V = 0.5$ mm/s, and $G = 80G_0$ (stiff shear plate). The general dynamics of these two periods are shown in Fig. 3f. $|V_{xt}|$ and $|V_{xb}|$ represent the absolute values of the velocity of sensors on the top and bottom plate, respectively, and the deeper the colour, the larger the value. (a) Plate motion of the model with soft plates. (b) Plate motion of the model with stiff plates. (c) Plastic flow of a typical large slip event in the model sheared by soft plates. The orange arrow indicates the source of the event. (d) Plastic flow of a typical large slip event sheared by stiff plates. The black arrow indicates the source of the event.

our numerical model simulating substantial slips, the coseismic slips between shear plate surfaces are confined to a millimeter scale (~1 mm), significantly less than the gouge thickness (~11 mm). Consequently, although our model's results do not directly mirror the dynamics of catastrophic natural earthquakes, they may offer valuable insights into the flow behavior of granular gouge interposed between fault surfaces during seismic events and the consequent stress redistribution patterns.

However, conducting a detailed simulation could yield comprehensive verification data for frictional constitutive models, thereby enhancing the accuracy of simulations involving natural faults. Engineering endeavors in geotechnics, including railway construction and tunnel maintenance, are intricately linked to the shearing behavior of natural faults [76]. By incorporating the granular inertia number I and the rate ratio J, Fei et al. [77] refined the classical Rate- and State-Friction law, allowing for a more physically accurate description; they calibrated the parameters of this updated law through laboratory experiments involving granular faults. Subsequently, integrating geological and project-specific data, they applied their model to geological-scale simulations of sheared faults. Their research elucidated how different fault types impact railway systems and assessed whether fault displacements exceeded established standards. Therefore, detailed simulations and analyses of laboratory-induced earthquakes have the potential to furnish comprehensive verification data for frictional constitutive models, thereby facilitating simulations at the engineering scale and providing crucial support for engineering projects associated with faults.

Here, to accurately depict the evolution of stress chain structures, we analyze stress redistribution by monitoring variations in the magnitude of maximum shear stress. Nevertheless, within the realm of Continuum Mechanics, the stress state is comprehensively described by tensors [78], which encompass a wealth of information, including stress magnitudes

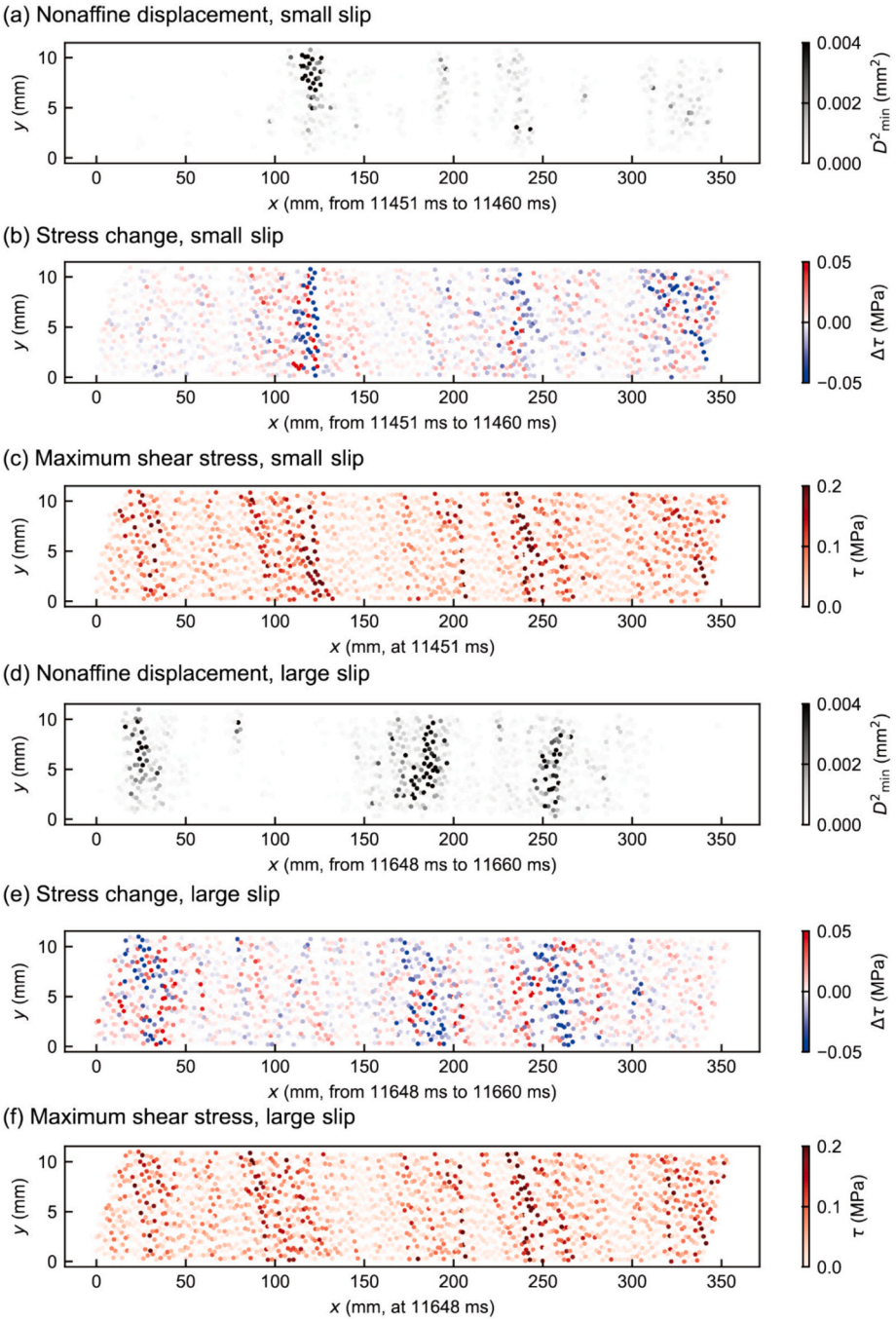

Fig. 13. The non-affine displacements and stresses of slip events. The two slip examples are taken from the model where $P = 28$ kPa, $V = 0.5$ mm/s, and $G = 4G_0$ (as marked in Fig. 6). (a) - (c) Spatial distributions of non-affine displacements, stress change and maximum shear stress of the small slip, respectively. (d) - (f) Spatial distributions of non-affine displacements, stress change and maximum shear stress of the large slip, respectively.

in various directions and the orientations of the maximum principal and shear stresses. Conducting a thorough statistical analysis of the stress tensor's evolution and its correlation with prior states could significantly enhance our comprehension of stress redistribution within granular gouge experiencing stick-slip cycles—a task that holds promise for future exploration [79].

Frye and Marone [80] undertook a series of laboratory experiments to juxtapose two-dimensional (2D) and three-dimensional (3D) models: the former involving the shearing of parallel cylindrical rods, and the latter, the shearing of spherical grains. Their results indicate that the shear strength demonstrated by the 2D model is inferior to that of the 3D counterpart. This variance can be ascribed to the absence of out-of-plane contacts in the 2D model. In contrast, within 3D models, stress redistribution transpires not only along the dip direction of faults but also along the strike direction. Future investigations could examine how the additional dimension affects stress redistribution in the 3D model and probe the disparities in stress redistribution between the 2D and 3D models. Furthermore, in natural faults, gouge grains undergo crushing during slip, with their size distribution adhering to a power law [81,82]. The intricate geometry of fault planes, irregular particle shapes, mineral heterogeneity [83,84], and the chemical reactions of minerals during shear also influence granular rearrangement [85]. Detailed studies exploring how these factors affect stress redistribution in granular faults could be conducted in the future.

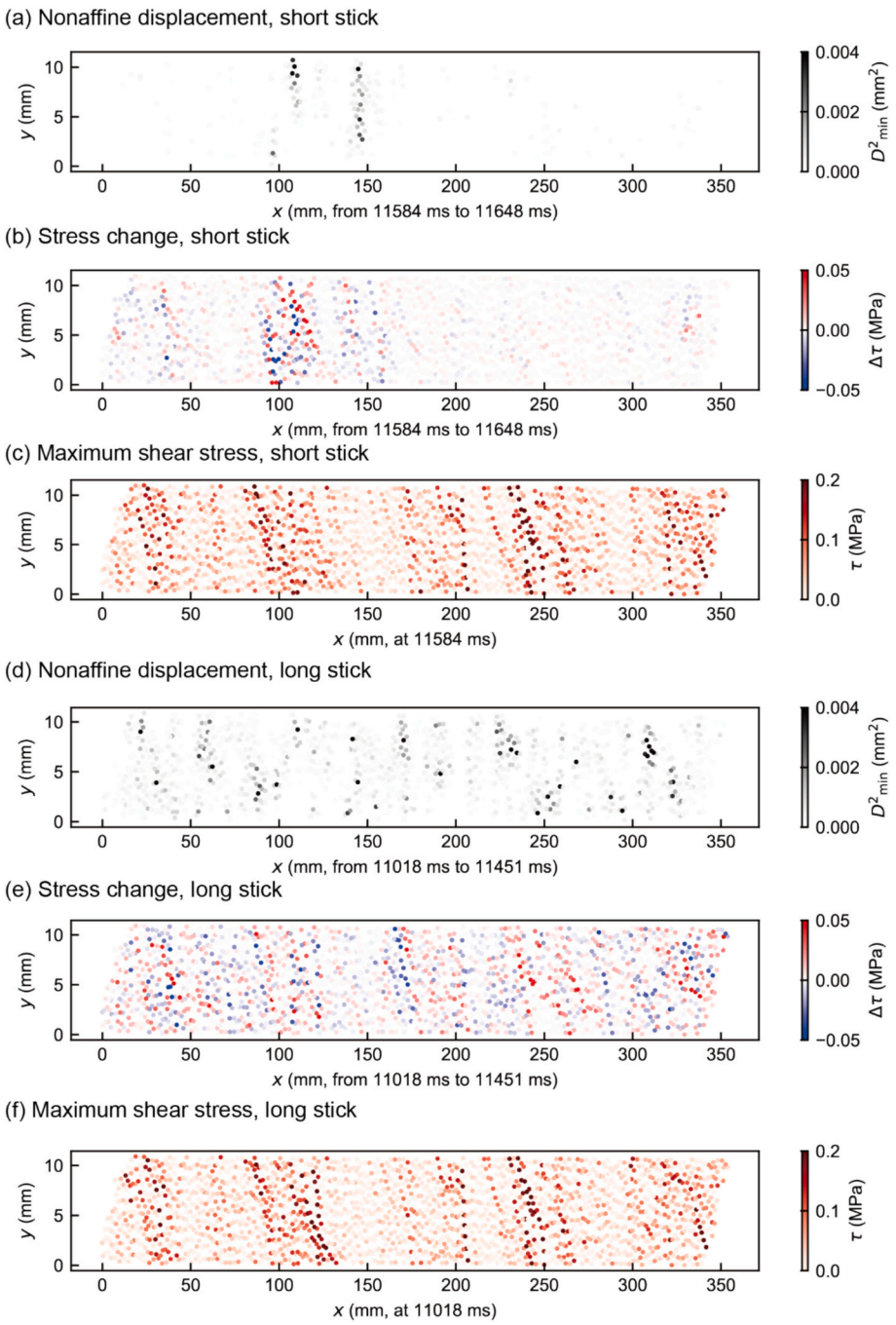

Fig. 14. The non-affine displacements and stresses of stick periods. The two stick examples are taken from the model where $P = 28$ kPa, $V = 0.5$ mm/s, and $G = 4G_0$ (marked in Fig. 6). (a) - (c) Spatial distributions of non-affine displacements, stress change and maximum shear stress of the short stick, respectively. (d) - (f) Spatial distributions of non-affine displacements, stress change and maximum shear stress of the long stick, respectively.

5. Conclusions

In this study, we simulate granular faults under different loading conditions. The increase in normal stress causes the granular faults to exhibit more pronounced stick-slip events, as well as the occurrence of fast slip events. When the shear velocity is much lower than the slip velocity, the increase of shear velocity results in more prominent stick-slip cycles, and the recurrence time of slip events is also shorter. Stiff plates produce slip events with lower slip velocities but larger seismic moments, and they also result in oscillatory shear force driven by stick-slip cycles.

The plastic granular flow during shearing and the effects of loading conditions on it are also discussed. The granular plasticity is strongly localized in small slips. In large slips, granular plasticity concentrates on several areas. Granular plasticity is also strongly localized in short sticks, whereas it is most homogeneous in long sticks. Higher normal stress, higher shear velocity, or lower plate stiffness results in more intense plastic flow of fault gouge during the slip phase, corresponding to faster slip events. The stiff plates intensify particle plastic flow in the stick phases and shorten the recurrence time. Due to the similar geometry of numerical granular faults, the distribution of granular plasticity, normalized by the total strain, is similar across all loading conditions.

The redistribution of stress in the thin granular gouge resulting from plastic granular flow is analyzed. When a slip event occurs, the stress on

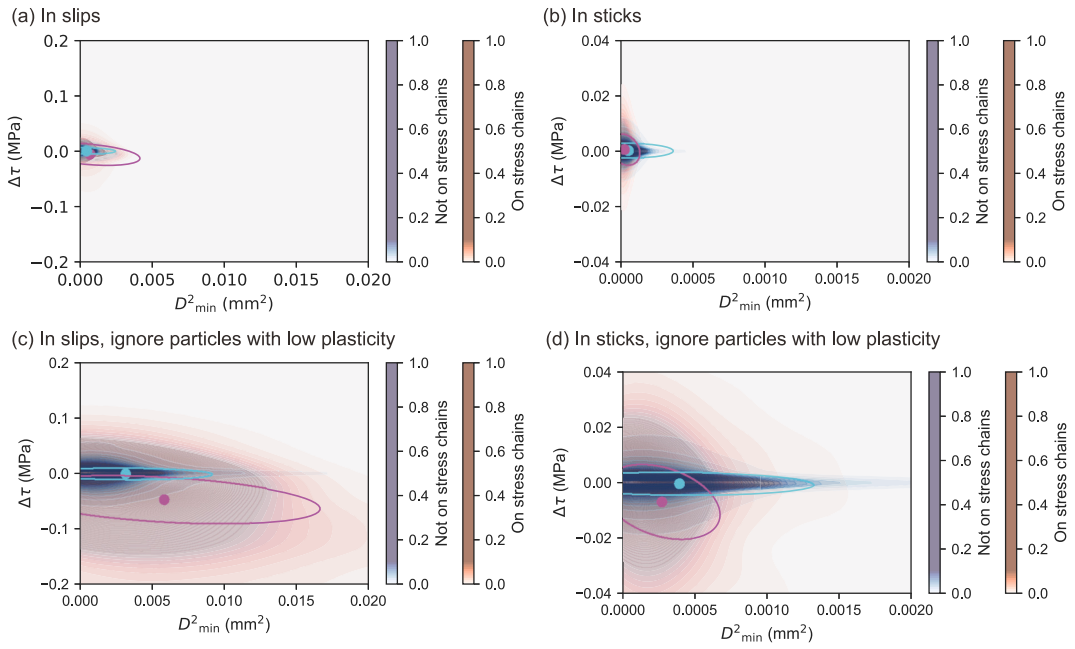

Fig. 15. Relationship between the non-affine displacement and stress change. The four pictures here show the normalized probability density in four different circumstances. The corresponding covariance error ellipses of the distribution of stress change and non-affine displacement are also plotted (magenta for particles on stress chains and cyan for particles not on stress chains). (a) and (b) are for slips and sticks, respectively. To characterize the effects caused by plastic flow, the top 10% particles with large non-affine displacement in each slip event or stick period are extracted, and the other particles with lower non-affine displacement are ignored. (c) and (d) ignore particles with low plasticity, and they are for slips and sticks, respectively. (For interpretation of the references to colour in this figure legend, the reader is referred to the web version of this article.)

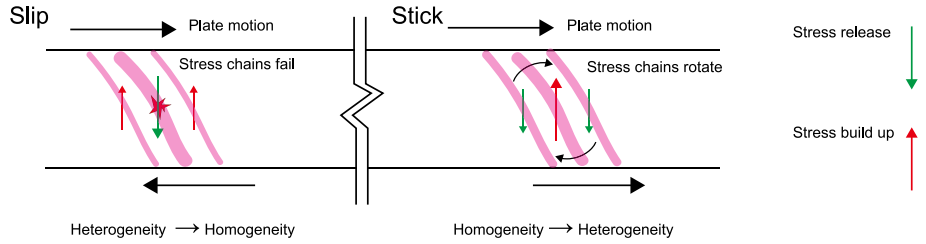

Fig. 16. Diagram of stress evolution. When a strong stress chain fails, slip events occur, decreasing the stress on that chain. The induced plate motion, in turn, increases the stress on nearby stress chains. On the contrary, in the stick phases, some stress chains rotate slightly to support the plates, and stress is built up on these stress chains; the stress near the rotating stress chains decreases.

the failed stress chain is released, increasing the stress in the surrounding stress chains and driving the stress state towards homogeneity. During the stick phase, the stress chains slowly rotate, thickening the gouge and accumulating stress, decreasing the surrounding stress state, and driving the system towards heterogeneity. This paper examines the 2D plastic flow characteristics under various loading conditions and the associated stress redistribution, thereby enhancing understanding of the plastic flow of granular gouge during shear in faults with uniform structures oriented perpendicular to the slip direction.

CRediT authorship contribution statement

Zhuan Dai: Writing – original draft, Visualization, Methodology, Investigation, Formal analysis, Data curation, Conceptualization. **Ke Gao:** Writing – review & editing, Validation, Supervision, Software, Resources, Project administration, Methodology, Conceptualization.

Declaration of competing interest

The authors declare that they have no known competing financial interests or personal relationships that could have appeared to influence the work reported in this paper.

Acknowledgments

This work is supported by the National Natural Science Foundation of China (42374070). Zhuan Dai analyzed the data and drafted the manuscript. Ke Gao carried out the numerical simulation and revised the manuscript. Zhuan Dai would like to acknowledge the Yunnan Provincial Department of Education Scientific Research Fund Project (2026J1046), Baoshan University Doctoral Research Startup Fund Program 2025 (BSKY2545), and Baoshan University Teaching Reform Project (ZHZ202602).

Appendix A. Supplementary data

Supplementary data to this article can be found online at https://doi.org/10.1016/j.powtec.2026.122759.

Data availability

The codes for extracting events, calculating non-affine displacement, and figuring can be found at https://github.com/xiaoDai4/Plastic-Flow-and-Stress-Redistribution-in-Sheared-Granular-Gouge

References

[1] T.M. Qu, J.D. Zhao, Y. Feng, Artificial intelligence for computational granular media, Comput. Geotech. 185 (2025), https://doi.org/10.1016/j.compgeo.2025.107310.

[2] N. Topic, F.M. Schaller, G.E. Schröder-Turk, T. Pöschel, The microscopic structure of mono-disperse granular heaps and sediments of particles on inclined surfaces, Soft Matter 12 (2016) 3184–3188, https://doi.org/10.1039/c5sm03114a.

[3] G.F. Ma, J.T. Kirby, T.J. Hsu, F.Y. Shi, A two-layer granular landslide model for tsunami wave generation: theory and computation, Ocean Model. 93 (2015) 40–55, https://doi.org/10.1016/j.ocemod.2015.07.012.

[4] A. Köhler, J.N. McElwaine, B. Sovilla, GEODAR data and the flow regimes of snow avalanches, J. Geophys. Res. Earth Surf. 123 (2018) 1272–1294, https://doi.org/10.1002/2017jf004375.

[5] J.J. Warmink, C.M. Dohmen-Janssen, J. Lansink, S. Naqshband, O.J.M. van Duin, A.J. Paarlberg, P. Termes, S. Hulscher, Understanding river dune splitting through flume experiments and analysis of a dune evolution model, Earth Surf. Process. Landf. 39 (2014) 1208–1220, https://doi.org/10.1002/esp.3529.

[6] X.B. Wang, N.R. Morgenstern, D.H. Chan, A model for geotechnical analysis of flow slides and debris flows, Can. Geotech. J. 47 (2010) 1401–1414, https://doi.org/10.1139/t10-039.

[7] J.H. Dieterich, Modeling of rock friction: 2. Simulation of preseismic slip, J. Geophys. Res. Solid Earth 84 (1979) 2169–2175, https://doi.org/10.1029/JB084iB05p02169.

[8] D.D. Kosloff, H.-P. Liu, Reformulation and discussion of mechanical behavior of the velocity-dependent friction law proposed by Dieterich, Geophys. Res. Lett. 7 (1980) 913–916, https://doi.org/10.1029/GL007i011p00913.

[9] J.H. Dieterich, Constitutive Properties of Faults With Simulated Gouge, in: Mechanical Behavior of Crustal Rocks, 1981, pp. 103–120.

[10] A. Ruina, Slip instability and state variable friction laws, J. Geophys. Res. Solid Earth 88 (1983) 10359–10370, https://doi.org/10.1029/JB088iB12p10359.

[11] C. Marone, Laboratory-derived friction laws and their application to seismic faulting, Annu. Rev. Earth Planet. Sci. 26 (1998) 643–696, https://doi.org/10.1146/annurev.earth.26.1.643.

[12] M.M. Scuderi, C. Collettini, C. Viti, E. Tinti, C. Marone, Evolution of shear fabric in granular fault gouge from stable sliding to stick slip and implications for fault slip mode, Geology (2017), https://doi.org/10.1130/g39033.1.

[13] Y. Xing, J. Zheng, J. Li, Y. Cao, W. Pan, J. Zhang, Y. Wang, X-Ray tomography investigation of cyclically sheared granular materials, Phys. Rev. Lett. 126 (2021) 048002, https://doi.org/10.1103/PhysRevLett.126.048002.

[14] J. Aubry, F.X. Passelegue, D. Deldicque, F. Girault, S. Marty, A. Lahfid, H.S. Bhat, J. Escartin, A. Schubnel, Frictional heating processes and energy budget during laboratory earthquakes, Geophys. Res. Lett. 45 (2018) 12274–12282, https://doi.org/10.1029/2018gl079263.

[15] M.J. Ikari, Y. Ito, K. Ujiie, A.J. Kopf, Spectrum of slip behaviour in Tohoku fault zone samples at plate tectonic slip rates, Nat. Geosci. 8 (2015) 870–874, https://doi.org/10.1038/ngeo2547.

[16] M. Acosta, F.X. Passelegue, A. Schubnel, M. Violay, Dynamic weakening during earthquakes controlled by fluid thermodynamics, Nat. Commun. 9 (2018) 3074, https://doi.org/10.1038/s41467-018-05603-9.

[17] F.X. Passelegue, J. Aubry, A. Nicolas, M. Fondriest, D. Deldicque, A. Schubnel, G. Di Toro, From fault creep to slow and fast earthquakes in carbonates, Geology 47 (2019) 744–748, https://doi.org/10.1130/G45868.1.

[18] M.J. Ikari, C. Marone, D.M. Saffer, On the relation between fault strength and frictional stability, Geology 39 (2011) 83–86, https://doi.org/10.1130/g31416.1.

[19] G. Pozzi, N. De Paola, S.B. Nielsen, R.E. Holdsworth, T. Tesei, M. Thieme, S. Demouchy, Coseismic fault lubrication by viscous deformation, Nat. Geosci. 14 (2021) 437–442, https://doi.org/10.1038/s41561-021-00747-8.

[20] G.C. McLaskey, Earthquake initiation from laboratory observations and implications for foreshocks, J. Geophys. Res. Solid Earth 124 (2019) 12882–12904, https://doi.org/10.1029/2019jb018363.

[21] F. Yamashita, E. Fukuyama, S.Q. Xu, K. Mizoguchi, H. Kawakata, S. Takizawa, Rupture preparation process controlled by surface roughness on meter-scale laboratory fault, Tectonophysics 733 (2018) 193–208, https://doi.org/10.1016/j.tecto.2018.01.034.

[22] S. Xu, E. Fukuyama, F. Yamashita, H. Kawakata, K. Mizoguchi, S. Takizawa, Fault strength and rupture process controlled by fault surface topography, Nat. Geosci. 16 (2023) 94–100, https://doi.org/10.1038/s41561-022-01093-z.

[23] K. Xia, A.J. Rosakis, Laboratory earthquakes along faults with a low velocity zone: directionality and pulse-like ruptures, Extr. Mech. Lett. 46 (2021), https://doi.org/10.1016/j.eml.2021.101321.

[24] L. Buijze, Y. Guo, A.R. Niemeijer, S. Ma, C.J. Spiers, Nucleation of stick-slip instability within a large-scale experimental fault: effects of stress heterogeneities due to loading and gouge layer compaction, J. Geophys. Res. Sol. Ea. 125 (2020), https://doi.org/10.1029/2019JB018429.

[25] F. Corbi, L. Sandri, J. Bedford, F. Funiciello, S. Brizzi, M. Rosenau, S. Lallemand, Machine learning can predict the timing and size of analog earthquakes, Geophys. Res. Lett. 46 (2019) 1303–1311, https://doi.org/10.1029/2018gl081251.

[26] F. Corbi, F. Funiciello, S. Brizzi, S. Lallemand, M. Rosenau, Control of asperities size and spacing on seismic behavior of subduction megathrusts, Geophys. Res. Lett. 44 (2017) 8227–8235, https://doi.org/10.1002/2017gl074182.

[27] F. Corbi, F. Funiciello, M. Moroni, Y. van Dinther, P.M. Mai, L.A. Dalguer, C. Faccenna, The seismic cycle at subduction thrusts: 1. Insights from laboratory models, J. Geophys. Res. Sol. Ea. 118 (2013) 1483–1501, https://doi.org/10.1029/2012jb009481.

[28] H. Lei, A.R. Niemeijer, Y. Zhou, C.J. Spiers, Frictional properties of natural granite fault gouge under hydrothermal conditions: a case study of strike-slip fault from Anninghe Fault Zone, Southeastern Tibetan Plateau, J. Geophys. Res. Solid Earth 129 (2024), https://doi.org/10.1029/2024jb028760.

[29] B.M. Carpenter, C. Marone, D.M. Saffer, Weakness of the San Andreas Fault revealed by samples from the active fault zone, Nat. Geosci. 4 (2011) 251–254, https://doi.org/10.1038/ngeo1089.

[30] M.M. Scuderi, E. Tinti, M. Cocco, C. Collettini, The role of shear fabric in controlling breakdown processes during laboratory slow-slip events, J. Geophys. Res. Solid Earth 125 (2020), https://doi.org/10.1029/2020jb020405.

[31] G. Pozzi, M.M. Scuderi, E. Tinti, M. Nazzari, C. Collettini, The role of fault rock fabric in the dynamics of laboratory faults, J. Geophys. Res. Solid Earth 127 (2022), https://doi.org/10.1029/2021jb023779.

[32] G. Pozzi, C. Collettini, M.M. Scuderi, T. Tesei, C. Marone, A. Amodio, M. Cocco, Fabric controls fault stability in serpentinite gouges, Geophys. J. Int. 235 (2023) 1778–1797, https://doi.org/10.1093/gji/ggad322.

[33] B. Kou, Y. Cao, J. Li, C. Xia, Z. Li, H. Dong, A. Zhang, J. Zhang, W. Kob, Y. Wang, Granular materials flow like complex fluids, Nature 551 (2017) 360–363, https://doi.org/10.1038/nature24062.

[34] Y. Cao, J. Li, B. Kou, C. Xia, Z. Li, R. Chen, H. Xie, T. Xiao, W. Kob, L. Hong, J. Zhang, Y. Wang, Structural and topological nature of plasticity in sheared granular materials, Nat. Commun. 9 (2018) 2911, https://doi.org/10.1038/s41467-018-05329-8.

[35] K.E. Daniels, N.W. Hayman, Force chains in seismogenic faults visualized with photoelastic granular shear experiments, J. Geophys. Res. Solid Earth 113 (2008), https://doi.org/10.1029/2008jb005781.

[36] V. Chikkadi, P. Schall, Nonaffine measures of particle displacements in sheared colloidal glasses, Phys. Rev. E 85 (2012), https://doi.org/10.1103/PhysRevE.85.031402.

[37] Y. Zou, G. Ma, J. Mei, J. Zhao, W. Zhou, Microscopic origin of shape-dependent shear strength of granular materials: a granular dynamics perspective, Acta Geotech. 17 (2021) 2697–2710, https://doi.org/10.1007/s11440-021-01403-6.

[38] B. Ferdowsi, M. Griffa, R.A. Guyer, P.A. Johnson, C. Marone, J. Carmeliet, Microslips as precursors of large slip events in the stick-slip dynamics of sheared granular layers: a discrete element model analysis, Geophys. Res. Lett. 40 (2013) 4194–4198, https://doi.org/10.1002/grl.50813.

[39] Y. Zhao, Y. Zhao, D. Wang, H. Zheng, B. Chakraborty, J.E.S. Socolar, Ultrastable shear-jammed granular material, Phys. Rev. X 12 (2022), https://doi.org/10.1103/PhysRevX.12.031021.

[40] B. Ferdowsi, M. Griffa, R.A. Guyer, P.A. Johnson, C. Marone, J. Carmeliet, Three-dimensional discrete element modeling of triggered slip in sheared granular media, Phys. Rev. E Stat. Nonlinear Soft Matter Phys. 89 (2014) 042204, https://doi.org/10.1103/PhysRevE.89.042204.

[41] E. Aharonov, D. Sparks, Rigidity phase transition in granular packings, Phys. Rev. E 60 (1999) 6890–6896, https://doi.org/10.1103/PhysRevE.60.6890.

[42] E. Aharonov, D. Sparks, Shear profiles and localization in simulations of granular materials, Phys. Rev. E 65 (2002) 051302, https://doi.org/10.1103/PhysRevE.65.051302.

[43] E. Aharonov, D. Sparks, Stick-slip motion in simulated granular layers, J. Geophys. Res. Solid Earth 109 (2004), https://doi.org/10.1029/2003jb002597.

[44] S. Abe, K. Mair, Effects of gouge fragment shape on fault friction: new 3D modelling results, Geophys. Res. Lett. 36 (2009), https://doi.org/10.1029/2009gl040684.

[45] K. Mair, S. Abe, 3D numerical simulations of fault gouge evolution during shear: grain size reduction and strain localization, Earth Planet. Sci. Lett. 274 (2008) 72–81, https://doi.org/10.1016/j.epsl.2008.07.010.

[46] Z. Dai, K. Gao, Induced collective response in sheared granular faults exhibiting stick–slip, Granul. Matter 27 (2025) 49, https://doi.org/10.1007/s10035-025-01525-8.

[47] Z. Dai, K. Gao, J. Shang, Evolution of the principal slip zone in sheared granular faults, J. Geophys. Eng. 22 (2025) 743–759, https://doi.org/10.1093/jge/gxaf036.

[48] Z. Dai, K. Gao, J. Shang, Formation and evolution of shear structures in sheared granular gouge, Geophys. J. Int. 242 (2025), https://doi.org/10.1093/gji/ggaf164.

[49] A. Munjiza, The Combined Finite-Discrete Element Method, John Wiley & Son, Ltd, Lundon, 2004.

[50] Yu, Discrete element method, Eng. Comput. 21 (2004) 205–214, https://doi.org/10.1108/02644400410519749.

[51] B. Ferdowsi, A.M. Rubin, Slide-hold-slide protocols and frictional healing in Discrete Element Method (DEM) simulations of granular fault gouge, J. Geophys. Res. Sol. Ea. 126 (2021), https://doi.org/10.1029/2021jb022125.

[52] O. Dorostkar, J. Carmeliet, Grain friction controls characteristics of seismic cycle in faults with granular gouge, J. Geophys. Res. Solid Earth 124 (2019) 6475–6489, https://doi.org/10.1029/2019jb017374.

[53] T. Man, P. Zhang, Z. Ge, S.A. Galindo-Torres, Friction-dependent rheology of dry granular systems, Acta Mech. Sinica (2021) 1–11, https://doi.org/10.1007/s10409-021-0xxxx-x.

[54] Y. Guo, J.K. Morgan, Fault gouge evolution and its dependence on normal stress and rock strength—Results of discrete element simulations: gouge zone properties, J. Geophys. Res. Solid Earth 112 (2007), https://doi.org/10.1029/2006jb004524.

[55] K. Gao, B.J. Euser, E. Rougier, R.A. Guyer, Z. Lei, E.E. Knight, J. Carmeliet, P. A. Johnson, Modeling of stick-slip behavior in sheared granular fault gouge using the combined finite-discrete element method, J. Geophys. Res. Solid Earth 123 (2018) 5774–5792, https://doi.org/10.1029/2018jb015668.
[56] K. Gao, R.A. Guyer, E. Rougier, P.A. Johnson, Plate motion in sheared granular fault system, Earth Planet. Sci. Lett. 548 (2020), https://doi.org/10.1016/j.epsl.2020.116481.
[57] Y. Zhang, K. Gao, C. Li, Two Slip Regimes in Sheared Granular Fault, Earth Planet. Sci. Lett. 608 (2023), https://doi.org/10.1016/j.epsl.2023.118086.
[58] G. Mollon, J. Aubry, A. Schubnel, Laboratory Earthquakes Simulations-Typical Events, Fault Damage, and Gouge Production, J. Geophys. Res. Sol. Ea. 128 (2023), https://doi.org/10.1029/2022jb025429.
[59] P. Leishangthem, A.D.S. Parmar, S. Sastry, The yielding transition in amorphous solids under oscillatory shear deformation, Nat. Commun. 8 (2017) 14653, https://doi.org/10.1038/ncomms14653.
[60] G. Ma, Y. Zou, Y. Chen, L. Tang, T.-t. Ng, W. Zhou, Spatial correlation and temporal evolution of plastic heterogeneity in sheared granular materials, Powder Technol. 378 (2021) 263–273, https://doi.org/10.1016/j.powtec.2020.09.053.
[61] J. Mei, G. Ma, L. Tang, K. Gao, W. Cao, W. Zhou, Spatial clustering of microscopic dynamics governs the slip avalanche of sheared granular materials, Int. J. Plast. 163 (2023) 103570, https://doi.org/10.1016/j.ijplas.2023.103570.
[62] W.F. Brace, J.D. Byerlee, Stick-slip as a mechanism for earthquakes, Science 153 (1966) 990–991, https://doi.org/10.1126/science.153.3739.990.
[63] H. Kanamori, E.E. Brodsky, The Physics of earthquakes, Phys. Today 54 (2001) 34–40, https://doi.org/10.1063/1.1387590.
[64] H. Liu, H. Si, Z. Yang, D. Xu, Stress redistribution and crack evolution during fault slip: insights from coupled finite-discrete element method simulations, Phys. Fluids 37 (2025), https://doi.org/10.1063/5.0270195.
[65] Q. Liang, Z. Song, G. Huang, X. Huang, Y. Lu, J. Yao, G. Cheng, Influence of lateral stress on stick-slip characteristics of granite fault: a true three-dimensional experimental study, Phys. Fluids 37 (2025), https://doi.org/10.1063/5.0272823.
[66] K. Gao, R. Guyer, E. Rougier, C.X. Ren, P.A. Johnson, From stress chains to acoustic emission, Phys. Rev. Lett. 123 (2019) 048003, https://doi.org/10.1103/PhysRevLett.123.048003.
[67] D.A. Geller, R.E. Ecke, K.A. Dahmen, S. Backhaus, Stick-slip behavior in a continuum-granular experiment, Phys. Rev. E Stat. Nonlinear Soft Matter Phys. 92 (2015) 060201, https://doi.org/10.1103/PhysRevE.92.060201.
[68] J.C. Tsai, G.A. Voth, J.P. Gollub, Internal granular dynamics, shear-induced crystallization, and compaction steps, Phys. Rev. Lett. 91 (2003), https://doi.org/10.1103/PhysRevLett.91.064301.
[69] C. Marone, The effect of loading rate on static friction and the rate of fault healing during the earthquake cycle, Nature 391 (1998) 69–72, https://doi.org/10.1038/34157.
[70] J.R. Leeman, D.M. Saffer, M.M. Scuderi, C. Marone, Laboratory observations of slow earthquakes and the spectrum of tectonic fault slip modes, Nat. Commun. 7 (2016) 11104, https://doi.org/10.1038/ncomms11104.
[71] A. Niemeijer, C. Marone, D. Elsworth, Fabric induced weakness of tectonic faults, Geophys. Res. Lett. 37 (2010) 1–5, https://doi.org/10.1029/2009gl041689.
[72] J.H. Dieterich, Time-dependent friction and the mechanics of stick-slip, Pure Appl. Geophys. 116 (1978) 790–806, https://doi.org/10.1007/BF00876539.
[73] E.D. Cubuk, R.J.S. Ivancic, S.S. Schoenholz, D.J. Strickland, A. Basu, Z.S. Davidson, J. Fontaine, J.L. Hor, Y.-R. Huang, Y. Jiang, N.C. Keim, K.D. Koshigan, J.A. Lefever, T. Liu, X.-G. Ma, D.J. Magagnosc, E. Morrow, C.P. Ortiz, J.M. Rieser, A. Shavit, T. Still, Y. Xu, Y. Zhang, K.N. Nordstrom, P.E. Arratia, R.W. Carpick, D.J. Durian, Z. Fakhraai, D.J. Jerolmack, D. Lee, J. Li, R. Riggleman, K.T. Turner, A.G. Yodh, D. S. Gianola, A.J. Liu, Structure-property relationships from universal signatures of plasticity in disordered solids, Science 358 (2017) 1033–1037, https://doi.org/10.1126/science.aai8830.
[74] X. Ding, S. Xu, L. Ye, Intermittent supershear rupture punctuated by barrier-induced stopping phase during the 2025 Mw 7.8 Myanmar earthquake: evidence from near-fault strong motion observation, Geophys. Res. Lett. 52 (2025) e2025GL118863, https://doi.org/10.1029/2025GL118863.
[75] Z. He, Z. Zhang, X. Wang, Z. Wang, T.C. Sunilkumar, X. Xu, R. Wang, Rupture Dynamics of the 2025 Mw 7.7 Myanmar Earthquake: a Bilateral Supershear Rupture on Unusually Long Fault Superhighway, Geophys. Res. Lett. 53 (2026) e2025GL118023, https://doi.org/10.1029/2025GL118023.
[76] J. Fei, J. Wei, M.I. Khalid, X. Zhou, G. Li, X. Chen, Failure of Daliang tunnel induced by active stick–slip fault, J. Rock Mech. Geotech. Eng. 17 (2025) 3711–3725, https://doi.org/10.1016/j.jrmge.2024.07.007.
[77] J. Fei, R. Chen, X. Zhou, J. Wei, X. Chen, Response of railway embankment crossing active fault, Transp. Geotech. 55 (2025), https://doi.org/10.1016/j.trgeo.2025.101683.
[78] M. Epstein, Continuum mechanics, in: M.D. Binder, N. Hirokawa, U. Windhorst (Eds.), Encyclopedia of Neuroscience, Springer, Berlin Heidelberg, Berlin, Heidelberg, 2009.
[79] J.-T. Xue, Y. Bai, L. Peng, X.-B. Huang, Z.-Y. Sun, Exploring the interplay between local chain structure and stress distribution in polymer networks, Chin. J. Polym. Sci. 42 (2024) 874–885, https://doi.org/10.1007/s10118-024-3099-3.
[80] K.M. Frye, C. Marone, The effect of particle dimensionality on granular friction in laboratory shear zones, Geophys. Res. Lett. 29 (2002) 22-21–22-24, https://doi.org/10.1029/2002GL015709.
[81] A. Billi, Grain size distribution and thickness of breccia and gouge zones from thin (<1m) strike-slip fault cores in limestone, J. Struct. Geol. 27 (2005) 1823–1837, https://doi.org/10.1016/j.jsg.2005.05.013.
[82] C. Sammis, G. King, R. Biegel, The kinematics of gouge deformation, Pure Appl. Geophys. 125 (1987) 777–812, https://doi.org/10.1007/BF00878033.
[83] W.L. Power, T.E. Tullis, S.R. Brown, G.N. Boitnott, C.H. Scholz, Roughness of Natural Fault Surfaces, Geophys. Res. Lett. 14 (1987) 29–32, https://doi.org/10.1029/GL014i001p00029.
[84] Y. Tal, D. Faulkner, The effect of fault roughness and earthquake ruptures on the evolution and scaling of fault damage zones, J. Geophys. Res. Sol. Ea. 127 (2022), https://doi.org/10.1029/2021JB023352.
[85] G. Mollon, J. Aubry, A. Schubnel, Simulating melting in 2D seismic fault gouge, J. Geophys. Res. Solid Earth 126 (2021) e2020JB021485, https://doi.org/10.1029/2020JB021485.